Phosvitin phosphopeptides produced by pressurized hea-trypsin hydrolysis promote the differentiation and mineralization of MC3T3-E1 cells via the OPG/RANKL signaling pathways

Mengdie Zhao,* Shanshan Li,* Dong Uk Ahn,† and Xi Huang*,[1]

*National Research and Development Center for Egg Processing, College of Food Science and Technology, Huazhong Agricultural University, Wuhan, Hubei 430070, PR China; and †Animal Science Department, Iowa State University, Ames, USA

ABSTRACT Phosvitin (**PV**) from egg yolk is an excellent substrate for the production of phosphopeptides, which have a strong calcium chelating capacity and promoting calcium absorption and bone mineralization. This study investigated the effect of PV hydrolysates produced using a effective preparation method (high temperature (121°C) and mild pressure (0.1 MPa), HTMP) or HTMP pretreatment and trypsin hydrolysis combination (HTMP-PV18) on the physiology of an osteoblast MC3T3-E1 cells line. The proliferation, apoptosis, and differentiation of MC3T3-E1 cells were analyzed using the CCK-8, flow cytometry, and RT-PCR reactions, respectively. Both the HTMP-PV and HTMP-PV18 increased the proliferation, and inhibited the apoptosis of MC3T3-E1 cells significantly. The HTMP-PV increased the proliferation of MC3T3-E1 cells by 147.12 ± 2.11% and the HTMP-PV18 by 136.43 ± 4.51%. In addition, the HTMP-PV and HTMP-PV18 effectively promoted the expression of genes related to the OPG/RANKL signaling channel during cell differentiation. This indicated that both the HTMP-PV and HTMP-PV18 have the potential to promote bone mineralization by improving the proliferation and differentiation of osteoblastic cells.

Key words: phosvitin phosphopeptides, bone mineralization, high temperature and mild pressure, OPG/RANKL signaling channel, MC3T3-E1 cells

2021 Poultry Science 100:527–536
https://doi.org/10.1016/j.psj.2020.10.053

INTRODUCTION

Osteoporosis is a common skeletal disease in elderly women and causes a decrease in bone density that results in bone fractures (Woo et al., 2009). It is mainly caused by the imbalance between the bone calcium absorption and loss, where the osteoclastic activity is higher than the osteoblastic, although the loss of other elements such as phosphorus, magnesium, manganese are also involved (An et al., 2016). Therefore, the best treatment for osteoporosis is inhibiting the activity of osteoclastic cells while promoting the differentiation of the osteoblastic cells. The differentiation of osteoblastic cells can be modulated through several signaling pathways (i.e., BMP-SMAD, Wnt/β-catenin, and OPG/RANKL pathways). The bone morphogenetic protein-2 (BMP-2), a local growth factor, induces bone tissue formation and repair at the site of the fracture damages (Wang et al., 2014). Osteoprotegerin (**OPG**) inhibits the formation, differentiation, and survival of osteoclasts, and induces the apoptosis of osteoclasts. The receptor activator of nuclear factor-κB ligand (**RANKL**) is a factor required for the differentiation process of osteoclasts. However, when the OPG and RANKL are combined, they can inhibit the formation and activation of osteoclasts indirectly (Xia et al., 2015). The OPG/RANKL ratio is a critical signaling pathway that regulates the differentiation of osteoblasts. In this pathway, the expression of OPG and RANKL could be regulated by various factors, but an increase in the ratio of OPG/RANKL inhibits the function of osteoclast (Wu et al., 2017). Li et al. (2012) found that echinacoside, a natural phenol, could promote the proliferation and differentiation of osteoblasts by upregulating the rate of OPG/RANKL. Osteoporosis brings a great deal of inconvenience to the patients and generates physical and psychological pains. The bones of osteoporotic patients are fragile, and can be fractured easily. Once a patient has

Received August 24, 2020.
Accepted October 27, 2020.

[1]Corresponding author: huangxi@mail.hzau.edu.cn

fractured bones, they not only damage the health but also can be even life-threatening (Lunenfeld and Stratton, 2013). The treatment for osteoporosis is slow, and thus the prevention of osteoporosis is more important than the treatments. Many kinds of drugs are available to treat osteoporosis, but they generally have certain side effects and are not recommended for long-term use (Rachner et al., 2011). Therefore, finding biologically active substances that are capable of preventing osteoporosis with minimal side effects is important.

Bioactive peptides (**BAP**) are sequences of amino acids that are inactive within an original protein, but display specific physiological or biological activities in the body once they are released by enzymatic hydrolysis (Mora et al., 2014; Geng et al., 2017). The bioactive peptides derived from food proteins are excellent candidates for health-promoting agents because of their antioxidant, mineral-binding, immunomodulating and anticancer activities (Udenigwe and Aluko, 2012). Many studies have shown that phosphoproteins play important roles in the process of biomineralization because calcium binds to phosphate groups of phosphoproteins and promote mineral absorption and crystallization (Kwak et al., 2009). Jie et al. (2017) found that phosvitin, a major phosphoprotein in egg yolk, promoted the transformation of dicalcium phosphate dihydrate to hydroxyapatite and induced mineralization. Phosphopeptides derived from phosphoproteins also have the potentials to promote biomineralization. For example, casein phosphopeptides (**CPP**) are well-known phosphopeptides from milk and are widely used as a mineral absorption facilitator (Quarto et al., 2018). The CPP significantly promoted the absorption of calcium ions in the intestines and stomach of mice, and also promoted the process of bone deposition in vivo (Tsuchita et al., 2001). Donida et al. (2009) found that CPP stimulated calcium uptake by human osteoblast-like cells and upregulated the expression and the activity of alkaline phosphatase in osteoblasts.

Currently, casein is exclusively used to produce phosphopeptides commercially because it is cheap, easy to obtain (80% of total milk protein), and contains a few phosphoserine residues (1-13) in their structure depending on the type. However, phosvitin has a much greater number of phosphorylated amino acids in its structure than the casein. Phosvitin is composed of 217 amino acid residues of which 124 are serine residues and more than 90% of the serine residues in phosvitin are phosphorylated (Anton et al., 2006). Therefore, phosvitin can be an excellent source for phosphopeptide production with a great variety. Phosvitin phosphopeptides (**PPP**) were reported to have an ability to promote calcium and iron absorption in the intestinal tract because they form soluble calcium chelates instead of insoluble inorganic calcium salts (Choi et al., 2005; Zhong et al., 2016). However, the highly phosphorylated structure of phosvitin made it very difficult to produce phosphopeptides (Byrne et al., 1984). Over the years, various methods, including dephosphorylation (Mecham and Olcott, 1949), heat treatments, and high-pressure treatment (Volk et al., 2012), have been tested to improve the hydrolysis of phosvitin but with only limited success. However, our recent study indicated that high-temperature and mild pressure (**HTMP**) pretreatment and HTMP + enzyme combinations dramatically improved the degree of hydrolysis (**DH**) of phosvitin (Huang et al., 2019).

In this study, phosvitin was pretreated under HTMP conditions to open the PV structure and help the subsequent trypsin hydrolysis. The phosphopeptides produced using the HTMP and HTMP + trypsin were used to determine the effects of the phosphopeptides on the proliferation, apoptosis, and differentiation of osteoblastic MC3T3-E1 cells. The indices of cell proliferation activity such as the expression of BMP-2, OPG, and RANKL mRNA were used to determine the effect of PPP on the differentiation of the osteoblasts.

MATERIALS AND METHODS

Materials

Fresh eggs were purchased from the animal husbandry institute of Hubei Academy of Agricultural Sciences. The mouse pericranial bone-cell subclone 14 (osteoblastic MC3T3-E1 cell) was purchased from Shanghai Cell Bank of the Chinese Academy of Sciences (Shanghai, China).

Trypsin (E.C.3.4.4.4, ~15,500 U/mg protein), phosphate-buffered saline (**PBS**) were all purchased from the Sigma-Aldrich (St. Louis, MO); Tris-Tricine-SDS-PAGE gel electrophoresis kit was from Google Biology Limited (Wuhan, China); NaOH, HCl, ninhydrin, $CaCl_2$, 4% paraformaldehyde and 0.1% Alizarin-Red staining solution were all from Sinopharm Chemical Reagent Co., Ltd. (Nanjing, China); Cell Counting Kit-8 (**CCK-8**) was bought from Beijing Zoman Biotechnology Co., Ltd. (Beijing, China); 0.25% trypsin-EDTA were obtained from GIBCO (Australia); TRIzol, oligo, dNTPs, HiScript were all bought from Ambion (TX).

Pretreatment of Phosvitin

Phosvitin was prepared using the method of Lee et al. (2014) and treated as described below in accordance with the method of Huang et al. (2019) with some modifications: for the HTMP treatment, 10 mg/mL of phosvitin was dissolved in distilled water, the pH was adjusted to 6.5, and then subjected to 121°C, 0.1 MPa (HTMP) for 30 min (HTMP-PV) using an autoclave (Primus Sterilizer; Omaha, NE). Phosvitin was pretreated as described in the HTMP treatment, and added trypsin (1/50 enzyme/protein ratio, w/w) at pH 8.0, then incubated at 37°C for 18 h (HTMP-PV18). At the end of incubation, the enzyme was inactivated by heating the solution in a water bath at 100°C for 10 min, and then the hydrolysate was lyophilized.

Molecular Weight Distribution of the PV Hydrolysates

The molecular-size distribution of the phosvitin hydrolysates was determined using a 16.5% Tris-Tri

cine-SDS-PAGE gel electrophoresis. For the Tris-Tricine-SDS-PAGE analysis, the lyophilized samples were dissolved in distilled water at 2 mg/mL. The electrophoresis was run for 1 h at 30 V, and then the voltage was raised to 100 V and run until the bromophenol blue reached the bottom of the gel. The gel was stained using the Coomassie Brilliant Blue staining solution containing aluminum nitrate (0.1 mol) and then destained using an acetic acid–methanol solution.

Degree of Hydrolysis and the Calcium Chelation of PV and Its Hydrolysates

The DH of phosvitin hydrolysates (PV and HTMP-PV) was determined using the ninhydrin method (Chen and Ho, 1996). An aliquot of phosvitin hydrolysate (1 mL) was mixed with 1 mL of distilled water and 1 mL of ninhydrin, and boiled in a water bath for 15 min to generate a color. Then the solution was added with 5 mL of 40% ethanol and held for 15 min to measure the absorbance at 570 nm using a spectrophotometer (Beckman, Fullerton, CA).

The calcium chelation activity of the PV and HTMP-PV was measured using the atomic absorption method (Wang et al., 2018). Briefly, 1 mL of 0.1 mmol $CaCl_2$ solution was mixed with 10 mL of 1 mg/mL sample solution and incubated at 65°C for 2 h. After alcohol precipitation and centrifugation, the content of free calcium (C_0) in the supernatant was determined using an atomic absorption spectrophotometer. To determine total calcium content (C_t), 10 mL of distilled water was mixed with 1 mL of 0.1 mmol $CaCl_2$ solution. After centrifugation, the content of the total calcium (C_t) in the supernatant was determined.

$$\text{Calcium chelating rate } (\%) = \frac{(C_t - C_0)}{C_t} \times 100\%$$

Micromorphological Changes of the Hydrolyzed Products and Calcium-Chelating Peptides

About 2-4 mg of PV, HTMP-PV, or HTMP-PV18 powder was uniformly applied on a sample tray and then spray-coated with gold. The processed sample was placed on a scanning electron microscope, evacuated, and then scanned at 100× and 3,000× magnifications. The conditions of the scanning electron microscope were 15 kV, 6.9×10^{-2} mA, and 16.2 mm for pressure, beam current, and working distance, respectively.

Structural Characteristics of Phosvitin and Its Hydrolysates

Fluorescence spectroscopy was used to determine the structural characteristics of phosvitin and its hydrolysates (Wu et al., 2020). The sample powder was dissolved in distilled water (1 mg/mL) and subjected to an RF-5301 fluorescence spectrophotometer (Shimadzu Corp, Japan). The excitation and the emission wavelength were 280 and 300-500 nm, respectively, and the slit width was 5 nm. The infrared spectrum of phosvitin and its hydrolysate was recorded on the Perkin-Elmer 16 PC spectrometer (Boston, MA) at the wavelength range of 400-4,000 cm^{-1} with a resolution of 4.0 cm^{-1} and a scan of 32 times.

Cells Proliferation and Apoptosis Assay

Cell culture was done in accordance with the method of Jie et al. (2018). Four cell-culture media were prepared: ① control (cell-culture medium with no protein); ② phosvitin (cell-culture medium containing 100 μg/mL PV); ③ HTMP-PV (cell-culture medium containing 100 μg/mL HTMP-PV); and ④ HTMP-PV18 (cells-culture medium containing 100 μg/mL HTMP-PV18).

The proliferation activity of MC3T3-E1 osteoblastic cells was determined using the CCK-8 kit. The osteoblastic cells were seeded on a 96-well plate with 1×10^4 cells/well and then incubated at 37°C for 24 h. The cells were cultured another 24 h after applying the culture media prepared as above. The culture media were then replaced with 150 μL of a solution prepared with 9 mL culture medium +1 mL CCK-8, and the optical density was read using an Infinite M200 microplate reader (Swiss TECAN) at 450 nm after 2 h of incubation (Kim et al., 2014).

The apoptotic activity of MC3T3-E1 osteoblastic cells was determined using the flow cytometry. After seeding the cells (1×10^6 cells per well) on a 6-well plate, they were incubated in a cell incubator for 24 h, and then cultured for 24 h. The samples were centrifuged after digesting them with 0.25% trypsin-EDTA. The sediment was added with about 3 mL of PBS buffer (pH 7.0) and centrifuged at 1,100 × g for 5 min. The sediment was collected and washed 2 more times. Then, the sediment was added with 500 μL of a cell-loading buffer, 2 μL FITC and 5 μL propidium iodide, and then reacted for 15 min at room temperature. The apoptotic activity of the cells was determined using the flow cytometry.

RT-PCR of BMP-2, RANKL, and OPG mRNA

The mRNA of BMP-2, OPG, and RANKL were determined using the method described by Jie et al. (2018). A differentiation medium with or without phosvitin hydrolysates was added to the MC3T3-E1 cells and incubated for 3 d at 37°C. The expressions of BMP-2, OPG, and RANKL were analyzed using the RT-PCR reaction, with the GAPDH as a control. After incubation, the total RNA was extracted using the TRIzol Reagent (15596-026, Ambion) in accordance with the manufacturer's instruction. The cDNA was synthesized by incubating a solution containing 4.968 μg of total RNA, 2 μL of oligo (dT) 18, 4 μL of dNTPs, 1 μL of HiScript reverse transcriptase and 0.5 μL of ribonuclease inhibitor at 25°C for 5 min, 50°C for 15 min, 85°C for 5 min, and then 4°C for 10 min. Amplification was carried out for

40 cycles; the samples in a 20 μL reaction mixture containing 4 μL of cDNA, 10 μmol of each primer, 2.5 mmol dNTPs, and Taq Plus DNA Polymerase (ET105-01, TIANGEN) were incubated at 50°C for 2 min, 95°C for 10 min, 95°C for 30 s, and 60°C for 30 s. The primer sequences used are shown in Supplementary Table 1. The gene-expression values were calculated based on the comparative $2^{-\triangle\triangle Ct}$ method.

Analysis of the Mineralized Nodules of MC3T3-E1 Cells

The MC3T3-E1 cells (1×10^6 cells/well) were cultivated in a 6-well plate as described in 2.7. When the cells approached 80% confluence (denoted as day 0 of differentiation), 100 μg/mL PV, HTMP-PV, or HTMP-PV18 differentiation medium was added, and the medium was changed every 2 d. After 21 d of differentiation, the cells were washed with a precooled PBS buffer (4°C) 3 times and then added with a cell fixative (4% paraformaldehyde) to fix the cells at 4°C for 1 h. After washing with the PBS buffer, 200 μL of 0.1% Alizarin-Red staining solution (Sinopharm Chemical Reagent Co., Ltd., China) was added, and then stained for 30 min at room temperature. After rinsing with ultrapure water, the mineralized nodules of MC3T3-E1 were observed using a fluorescence inverted microscope (IX71, Olympus Co., Ltd., Japan). The quantitative analysis was shown by the drawing software (MATLAB 2016) referring to Jie et al. (2018). The formula is as follows:

$$\text{The proportion of mineralized nodules (\%)} = \frac{\text{value of the area of mineralized nodules}}{\text{value of the entire area of the image}}$$

Statistical Analysis

Data were analyzed using the SPSS 17.0 software. All experiments were repeated 3 times and the data were expressed as the mean ± SD. The data analysis was performed using the one-way analysis of variance followed by Duncan's post hoc test to find if significance was detected among the treatments. Statistical significance was set at $P < 0.05$. All Columnar patterns in this study were generated using the Origin 8.0 software.

RESULTS AND DISCUSSION

Molecular Weight Distribution of Phosvitin Phosphopeptides

The molecular weight of PV is about 35-40 kDa (Wallace and Morgan, 1986), and PV is highly resistant to proteases due to structure of high phosphorylation (Goulas et al., 1996; Samaraweera et al., 2014). Ren et al. (2015) reported that treatmenting of PV using 0.2 M NaOH for 30 min at room temperature partially dephosphorylated phosvitin and helped the subsequent trypsin digestion. However, the mineralization capability of the partially dephosphorylated PV was significantly lower than that of the natural PV (Jie et al., 2018). To reduce the protease resistance of PV without removing phosphate groups, pretreatment PV with high temperature under mild pressure condition (HTMP, 121°C at 1.5 atm) was developed by Huang et al. (2019). The structural characteristics of PV and its phosphopeptides were analyzed by liquid chromatography–tandem mass spectrometry. The HTMP pretreatment alone produced 154 peptides, whereas trypsin, Protex 6L, and Multifect14L combined HTMP pretreatment produced 225, 280, and 164 peptides, respectively (Huang et al., 2019). On this basis, this article investigated the activity and mechanism of PV hydrolysates produced by this effective method (HTMP and HTMP binding trypsin) on the differentiation and mineralization of osteoblasts.

The PV hydrolysates produced by trypsin enzymatic hydrolysis was mainly composed of 3 bands that are located near 40 kDa, 26 kDa, and below 17 kDa, and most of them are distributed above 20 kDa (Figure 1A). This indicated that the major proportion of phosvitin was not hydrolyzed. This result is consistent with the results in the above literatures. However, after HTMP pretreatment + trypsin enzymatic hydrolysis, the molecular weight of PV hydrolysates was mostly distributed below 15 kDa (Figure1B). When the enzymatic hydrolysis time was increased to >12 h, the molecular weight of most of the peptides in the hydrolysate was further reduced to <10 kDa (Figure 1B), indicating that the HTMP pretreatment destroyed the core structure of the PV and enabled the access of trypsin to further hydrolyze large peptides. Low-molecular-weight peptides were reported to be more conducive to calcium binding (Huang et al., 2014). For example, polypeptides with a molecular weight of 1-5 kDa have better calcium affinity than the larger ones (Lee and Song, 2009). In addition, small peptides are considered to be more suitable for intestinal absorption (Korhonen and Pihlanto, 2003). When the PV was pretreated with HTMP and then hydrolyzed with trypsin for 18 h, almost all the bands were located at < 10 kDa areas. Thus, PV, HTMP-PV, and HTMP-PV18 were selected for subsequent experiments (Figure 1B).

Microscopic Morphology Analysis of the PV and PV Hydrolysates With Chelated Calcium

The microstructure of PV showed a sheet-like structure with a smooth surface (Figure 2A), whereas that of the HTMP-PV had a broken, fragmented structure with some disorders and irregular shapes (Figure 2B). After

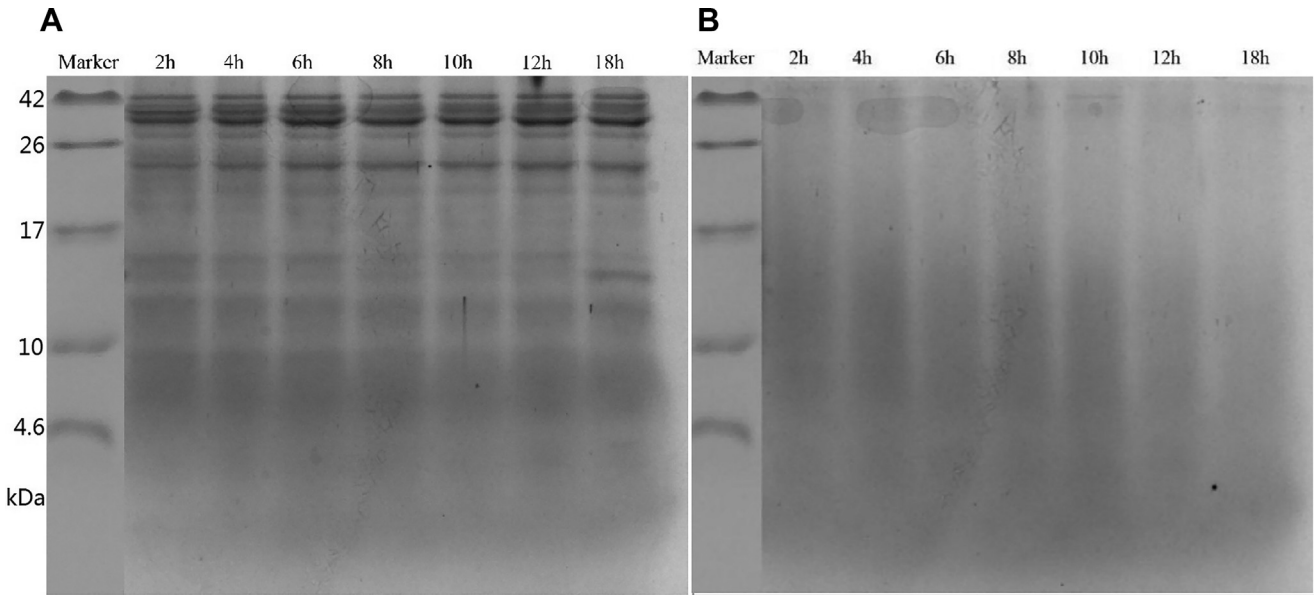

Figure 1. The Tris-Tricine-SDS-PAGE of phosvitin hydrolysates with trypsin (A) and PV hydrolysates with HTMP pretreatment and trypsin (B) with different incubation time. Abbreviations: HTMP-PV, high temperature and mild pressure pretreat phosvitin.

binding with calcium, the PV and HTMP-PV showed mineral-like structures (Figures 2C and 2D). Wang et al. (2017) reported that when calcium was bound to collagen polypeptides, many salt-like spherical aggregates appeared on the surface. This indicated that HTMP treatment destroyed the structure of PV, which was also confirmed by the DH (Figure 2E). The DH of PV increased from 3.32 to 18.06% ($P < 0.05$) after the HTMP pretreatment, indicating that the structure of PV was partially broken and more amino acids were exposed. The calcium

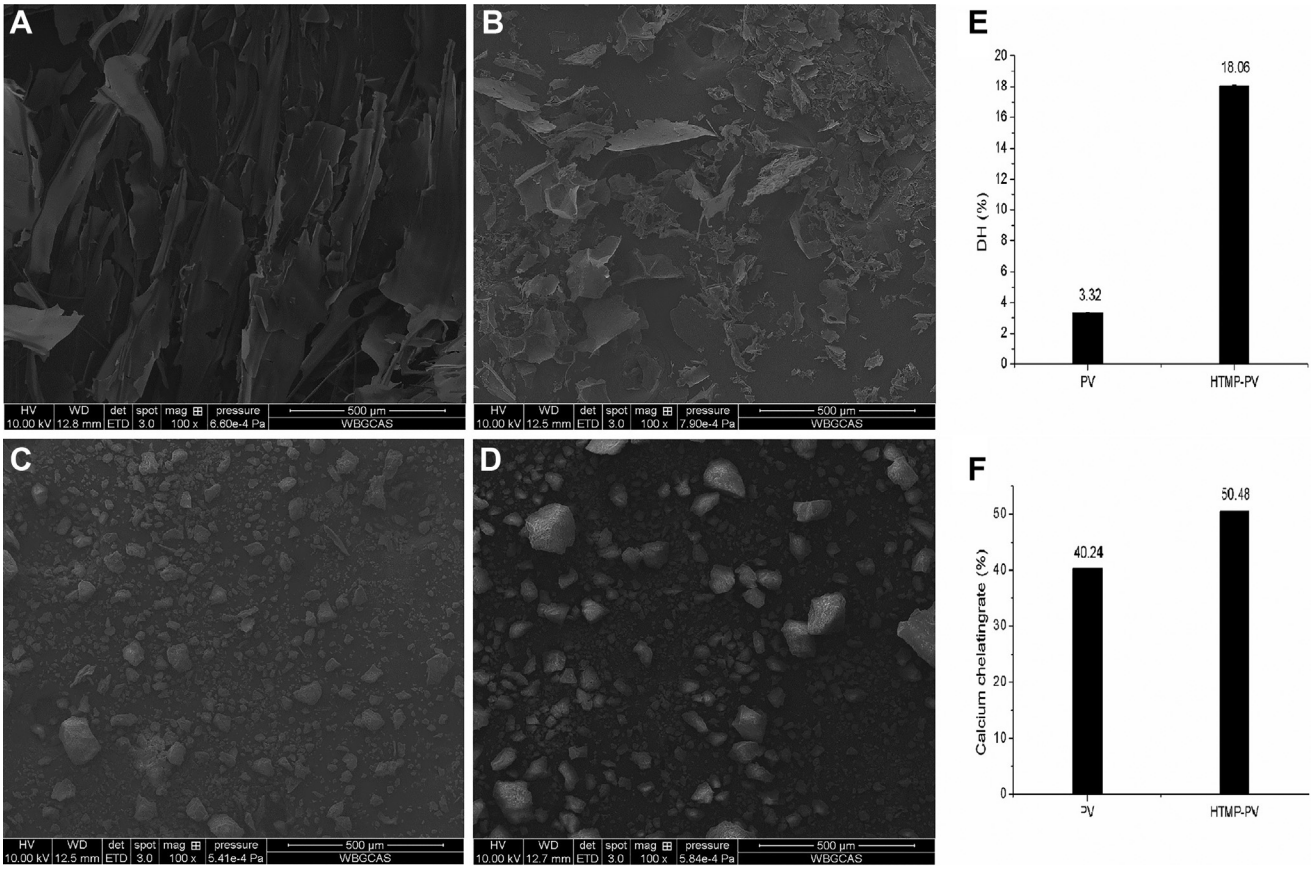

Figure 2. The scanning electron microscopic (SEM, 100x) images of the natural phosvitin and the HTMP pretreated phosvitin and their calcium chelates. A: phosvitin; B: high temperature and mild pressure pretreated phosvitin (HTMP-PV); C: phosvitin after calcium chelating; D: HTMP-PV after calcium chelating; E: the degree of hydrolysis of phosvitin and HTMP-PV; F: calcium chelating rate of phosvitin and HTMP-PV.

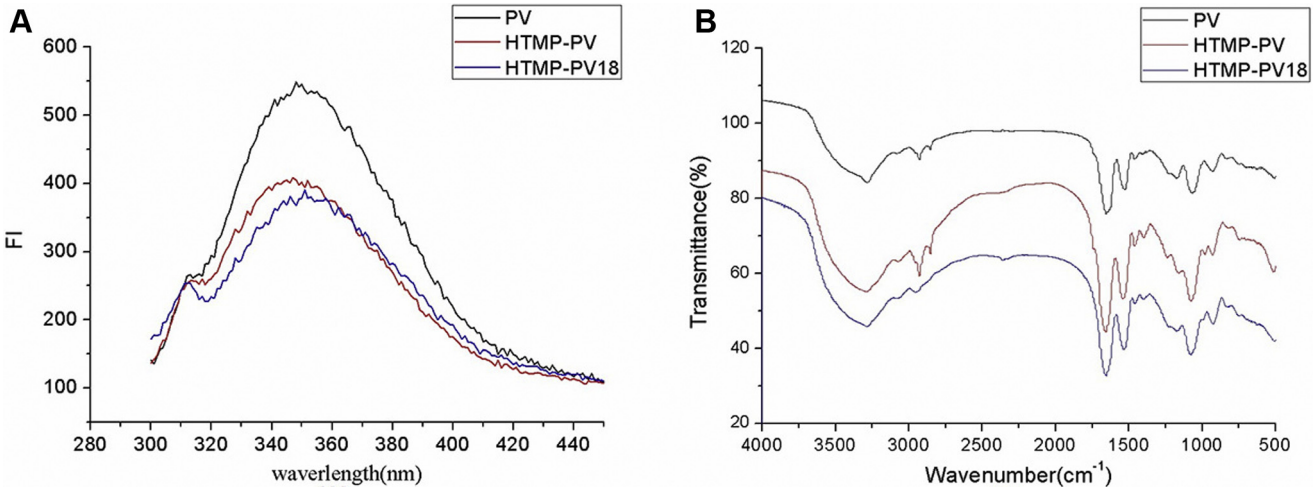

Figure 3. The fluorescence spectra (A) and Fourier infrared spectra (B) of the PV, HTMP-PV, and HTMP-PV18 (HTMP-PV: high temperature and mild pressure pretreated phosvitin; HTMP-PV18: HTMP-PV hydrolyzed with trypsin for 18 h).

binding rate of HTMP-PV was 50.48%, significantly higher than PV (40.24%) (Figure 2F) ($P < 0.05$), indicating that the structure of the PV was changed and some phosphorylated amino acid residues were exposed to bind more calcium.

Fluorescence Spectra and Fourier Infrared Spectra Analysis of PV and Its Hydrolysate

All 3 treatments (PV, HTMP-PV, and HTMP-PV18) showed the maximum fluorescence at 348 nm, but their intensities were different (Figure 3A). The changes in the absorption peak and the intensity of the absorption peak in the fluorescence spectrum at 348 nm reflect the changes in the environment where tryptophan is located (Zhao et al., 2011). The absorption intensity of the PV decreased after HTMP pretreatment and the spectrum had a slight red-shift, indicating that the polarity of tryptophan in the HTMP-PV had increased (Figure 3A). This indicated that the HTMP pretreatment changed the conformation of the PV, causing more chromophores to be exposed to the solution to undergo fluorescence quenching, which resulted in the decrease of fluorescence intensity.

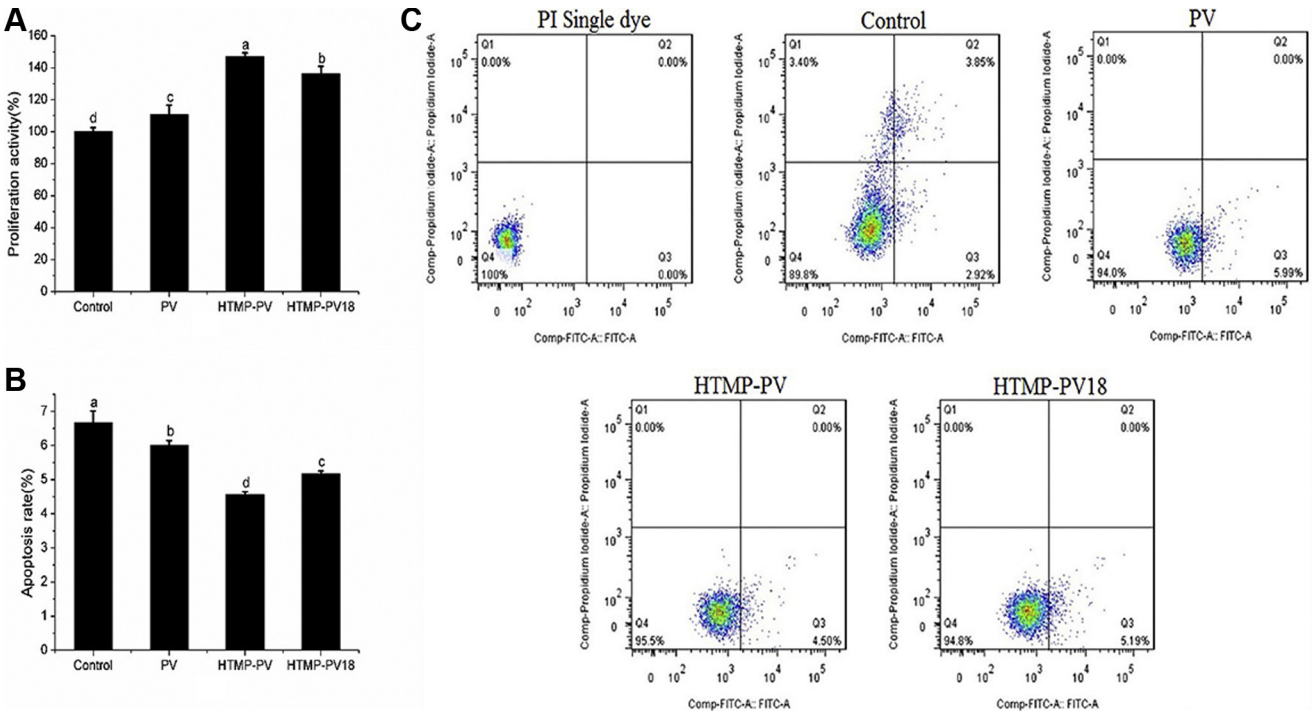

Figure 4. The effect of different treatment conditions of protein on the proliferation (A), apoptosis (B) and flow cytometer (C) of MC3T3-E1 cells (HTMP-PV: high temperature and mild pressure pretreated phosvitin; HTMP-PV18: HTMP-PV hydrolyzed with trypsin for 18 h). Data are expressed as mean SD (n = 6). Values marked with different letter are significantly different at $P < 0.05$.

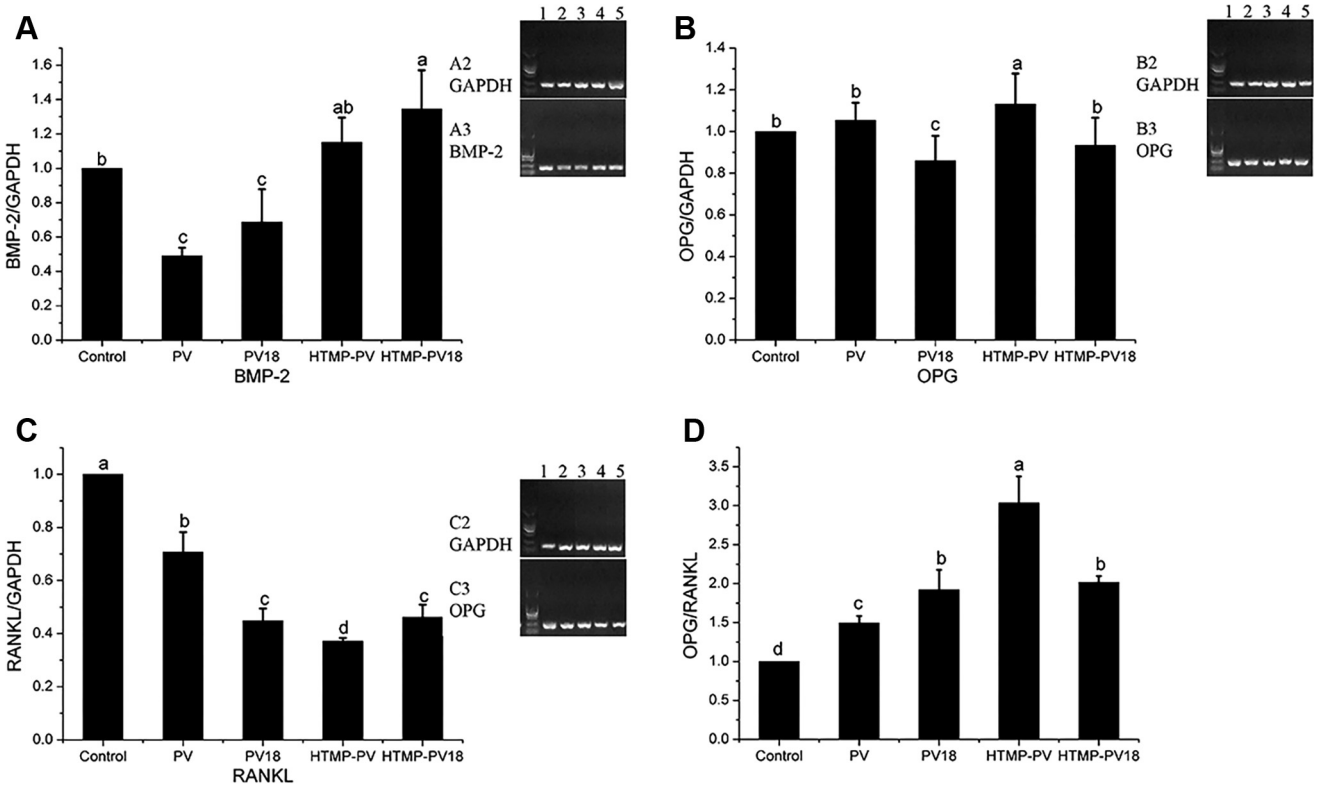

Figure 5. The expression level of BMP-2 (A), OPG (B), RANKL mRNA (C) and OPG/RANKL (D) analyzed using the real-time PCR. The samples were analyzed 3 d after adding the treatments. Figures A1, B1, and C1 are the gel electrophoresis of GAPDH (1: control; 2: phosvitin; 3:PV18; 4: HTMP-PV; 5: HTMP-PV18 treatment). The GAPDH mRNA level was analyzed in the same samples as the reference gene and visualized by the ethidium bromide stain on agarose gels. Results are expressed as the relative ratio to the control. Each value is the mean ± S.D. of 6 independent experiments. Data are expressed as mean SD (n = 6). Values marked with different letter are significantly different at $P < 0.05$.

The peak at 510 cm^{-1} in the IR spectrum of the PV is the bending vibration peak of PO_4^{3-} and that at 1,070 cm^{-1} is the asymmetric telescopic vibration peak of PO_4^{3-} (Figure 3B). This indicates that phosvitin is a phosphorylated protein. In the amide I band (1,600-1,700 cm^{-1}), there is a -C=O- stretching vibration peak at around 1,656 cm^{-1}. The absorption peak at 1,556 cm^{-1} belongs to the amide II band (1,600-1,500 cm^{-1}), which is produced by N-H in-plane bending and C-N stretching vibration. Compared with the infrared spectrum of the PV, the PO_4^{3-} bending vibration peak and the PO_4^{3-} asymmetric telescopic vibration peak of the HTMP-PV and the HTMP-PV18 did not change significantly. It is assumed that the HTMP pretreatment and the subsequent trypsin hydrolysis did not cause any changes in the phosphorylation of the PV. This is important for exploring the calcium-binding properties of the HTMP-PV and the HTMP-PV18. The characteristic absorption peak of the amide I band is caused by the C=O stretching vibration of the protein skeleton and is a sensitive region where the secondary structure of the protein changes. For both HTMP-PV and HTMP-PV18, the peak absorption wavelength of the amide I band shifted from 1,656 cm^{-1} to about 1,660 cm^{-1}, indicating that the secondary structure of the protein has changed and the proportion of α-helix has decreased.

Effects of HTMP-PV and HTMP-PV18 on the Proliferation and the Apoptosis of MC3T3-E1 Cells

All 3 treatments (PV, HTMP-PV, and HTMP-PV18) promoted the proliferation of MC3T3-E1 cells (Figure 4A). The proliferative activity of the HTMP-PV was 147.12% higher than that of the other groups ($P < 0.05$). The effect of PV in promoting cell proliferation was the lowest, which increased by only 10.82% compared with the control. With the HTMP pretreatment, the structure of the PV was partially broken and the phosphorylated serines in the core part were exposed and participated in biological reactions. It has been reported that the degree of phosphorylation in PV plays an important role in the proliferation and differentiation of MC3T3-E1 cells (Jie et al., 2018). The higher the degree of PV phosphorylation, the greater is the contribution of PV to the cell proliferation.

The apoptosis is an autonomous process that maintains the stability of the internal environment of cells and is controlled by genes. The HTMP-PV had the strongest inhibition effect on the apoptosis of MC3T3-E1 cells (4.56%), which was 31.63% lower than that of the control (Figure 4B) ($P < 0.05$). The apoptosis results were consistent with those of the cell proliferation (Figure 4C).

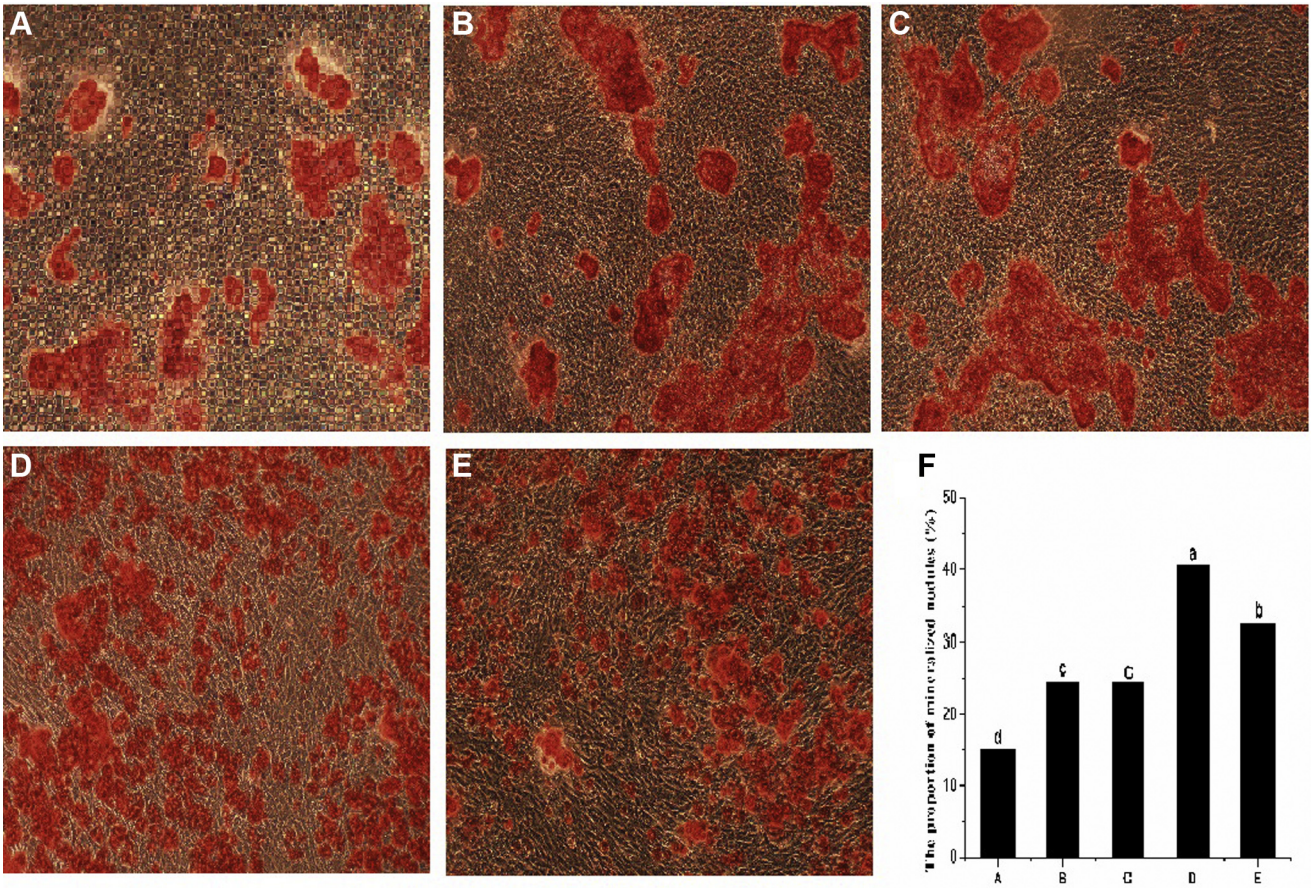

Figure 6. The effects of phosvitin with different hydrolysate treatments on the mineralized nodules of the MC3T3-E1 cells (demonstrated by the Alizarin-Red staining on day 21. Alizarin red complexes with calcium ions to form deep red substances) (A: control; B: phosvitin; C: PV18; D: HTMP-PV; E: HTMP-PV18; F: the proportion of mineralized nodules on A–E).

Expression of BMP-2, OPG, and RANKL mRNA Genes

The growth and development of the bones vary depending on the balance between the bone formation and the bone resorption. The major known signaling pathways of osteoblastic differentiation are OPG/RANKL (Jie et al., 2018), Wnt/β-catenin, 1,25-$(OH)_2$-vitaminD3/VDR (Kim et al., 2018), and BMP-SMAD. The proliferation and differentiation of osteoblasts occur at the same time as the osteoclasts are formed. The BMP-2 plays an important role in the bone formation. Ando et al. (2018) prepared a self-assembled peptide (SPG-178) that could significantly improve the level of BMP-2, osteocalcin, OPG, and other mRNA by in vitro as well as in vivo systems. In the OPG/RANKL rank system, cells secreted OPG, a protein involved in bone density regulation, to inhibit the development of osteoclasts. The stromal cells of bone marrow, as well as osteoblasts, secrete RANKL that promotes the differentiation of osteoclasts and bone resorption (Wang et al., 2014). In this study, the RT-PCR was used to detect marker genes such as BMP-2, OPG, and RANKL in OPG/RANKL signaling pathway of osteoblasts to determine the effect of phosvitin and its hydrolysates on cells differentiation.

The RT-PCR results of the bone mineralization–related genes indicated that the HTMP-PV and the HTMP-PV18 significantly upregulated the expression of BMP-2 mRNA, which was higher than that of PV and PV18 (phosvitin hydrolyzed by trypsin for 18 h) (Figure 5A1) ($P < 0.05$). Figure 1 showed that the molecular size of peptide from the enzymatically hydrolyzed phosvitin without pretreatment was greater than 10 kDa. From the RT-PCR, DH, and calcium chelation results, it was speculated that small peptides were more conducive to enter into the cells and promoted cell differentiation better than the large ones. The expression of OPG mRNA showed that the HTMP-PV and HTMP-PV18 upregulated the expression of OPG (Figure 5B1) but downregulated RANKL mRNA genes (Figure 5C1).

The activity of osteoblasts increased when the ratio of OPG to RANKL increased, which contributed to the bone formation. The OPG/RANKL values (Figure 5D) indicated that all 3 treatments increased the mineralization of osteoblasts, but the HTMP-PV showed the strongest effect. The activity of osteoclasts increased when the ratio of OPG/RANKL decreased, which favors bone resorption. Sritharan et al. (2018) reported that increasing OPG/RANKL ratio promoted the activity of osteoblasts by inhibiting osteoclastogenesis. The HTMP-PV and the HTMP-PV18 treatments promoted the differentiation of MC3T3-E1 cells significantly, but suppressed osteoclastogenesis by altering the OPG/RANKL ratio (Figure 5).

Effect of HTMP-PV and HTMP-PV18 on the Mineralized Nodules of MC3T3-E1 Cells

The formation of mineralized nodules is the hallmark of the advanced osteoblast differentiation, which occurs in the extracellular matrix (Li et al., 2019). The morphology, quantity, and size of the mineralized nodules are an intuitive morphological manifestation of cell mineralization. As shown in Figure 6, the mineralized nodules appeared in each group after the induced differentiation, and both the HTMP-PV and HTMP-PV18 had better mineralization effects than the control and the PV and PV18 groups (Figures 6A–6E) ($P < 0.05$). The quantitative analysis of mineralized nodules showed that the ratio of mineralized nodules in pretreated phosvitin groups was higher than that in the control group and no-pretreated groups (Figure 6F) ($P < 0.05$). Among them, the proportion of mineralized-nodule area in the HTMP-PV group was as high as 40.75%. This result indicated that the phosvitin after pretreatment is better in promoting mineralization of osteoblasts. Both the HTMP-PV and the HTMP-PV18 had a high calcium-chelating activity, which is beneficial to fix the calcium ions needed for the mineralization of the MC3T3E1 cells. Because the HTMP-PV and the HTMP-PV18 could contain many phosphorylated peptides, they can also provide phosphorus to the mineralized nodules. As reported by Jie et al. (2018), the PV with the high degree of phosphorylation (N75%) had a stronger effect in promoting the formation of osteoblast-mineralized nodules than that with the low-degree phosphorylation. 1 μg/mL Annatto-derived tocotrienol significantly increased expression of BMP-2 protein and mineralized calcium nodules were more abundant in Annatto-derived tocotrienol–treated groups than in the control (Hasan et al., 2020).

CONCLUSION

Both the HTMP-PV and the HTMP-PV18 treatments were effective in producing functional PPP from PV. The phosphopeptides produced from the HTMP-PV and the HTMP-PV18 treatments had higher calcium chelation, better osteoblasts differentiation, and mineralization rate than the phosvitin. The HTMP-PV and the HTMP-PV18 had stronger mineralization effects and osteoblasts differentiating effect than the control and the PV groups. The underlying mechanisms of the PPP in improving mineralization and the differentiation of osteoblast cells are by increasing the expression of the OPG/RANKL signaling-channel-related genes. Therefore, the PPP produced by the HTMP-PV and the HTMP-PV18 treatments could be promising anti-osteoporosis compounds for humans. However, producing PPP with strong calcium-chelating capacities and high osteoblasts differentiation and mineralization effects would be important for the practical application of the PPP to cure osteoporosis in the future. Therefore, further studies on the effects of peptide sizes, degree of phosphorylation, and amino acid sequences on the functional characteristics of PPP are necessary.

ACKNOWLEDGMENTS

This research was supported by the General Program of National Natural Science Foundation of China (grant number 32072237) and the National Key Research and Development Program of China (grant number 2018YFD0400302).

DISCLOSURES

The authors declare that they have no known competing financial interests or personal relationships that could have appeared to influence the work reported in this article.

SUPPLEMENTARY DATA

Supplementary data associated with this article can be found in the online version at https://doi.org/10.1016/j.psj.2020.10.053.

REFERENCES

An, J., H. Yang, Q. Zhang, C. Liu, J. Zhao, L. Zhang, and B. Chen. 2016. Natural products for treatment of osteoporosis: the effects and mechanisms on promoting osteoblast-mediated bone formation. Life Sci. 147:46–58.

Ando, K., S. Imagama, K. Kobayashi, K. Ito, M. Tsushima, M. Morozumi, S. Tanaka, M. Machino, K. Ota, K. Nishida, Y. Nishida, and N. Ishiguro. 2018. Effects of a self-assembling peptide as a scaffold on bone formation in a defect. PLoS One 13:1–12.

Anton, M., F. Nau, and Y. Nys. 2006. Bioactive egg components and their potential uses. Worlds Poult. Sci. J. 62:429–438.

Byrne, B. M., V. H. S. Ad, V. D. K. Ja, A. C. Arnberg, M. Gruber, and G. Ab. 1984. Amino acid sequence of phosvitin derived from the nucleotide sequence of part of the chicken vitellogenin gene. Biochemistry 23:4275–4279.

Chen, Q. Y., and C. T. Ho. 1996. Effect of amide content on thermal generation of maillard flavor in enzymatically hydrolyzed wheat protein. ACS Symp. Ser. 637:88–96.

Choi, I., C. Jung, H. Choi, C. Kim, and H. Ha. 2005. Effectiveness of phosvitin peptides on enhancing bioavailability of calcium and its accumulation in bones. Food Chem. 93:577–583.

Donida, B. M., E. Mrak, C. Gravaghi, I. Villa, S. Cosentino, E. Zacchi, S. Perego, A. Rubinacci, A. Fiorilli, G. Tettamanti, and A. Ferraretto. 2009. Casein phosphopeptides promote calcium uptake and modulate the differentiation pathway in human primary osteoblast-like cells. Peptides 30:2233–2241.

Geng, F., J. Q. Wang, D. Y. Liu, Y. G. Jin, and M. H. Ma. 2017. Identification of N-glycosites in chicken egg white proteins using an Omics Strategy. J. Agri. Food Chem. 65:5357–5364.

Goulas, A., E. L. Triplett, and G. Taborsky. 1996. Oligophosphopeptides of varied structural complexity derived from the egg phosphoprotein, phosvitin. J. Protein Chem. 15:1–9.

Hasan, W., N. Wan, K. Y. Chin, G. N. Abd, and I. N. Soelaiman. 2020. Annatto-derived Tocotrienol promotes mineralization of MC3T3-E1 cells by enhancing BMP-2 protein expression via inhibiting RhoA activation and HMG-CoA Reductase gene expression. Drug Des. Development Ther. 14:969–976.

Huang, H., B. F. Li, Z. Y. Liu, H. H. Wu, X. M. Mu, and M. Y. Zeng. 2014. Purification of a novel oligophosphopeptide with high calcium binding activity from carp egg hydrolysate. Food Sci. Technol. Res. 20:799–807.

Huang, X., S. H. Moon, J. Lee, H. Paik, E. J. Lee, B. Min, and D. U. Ahn. 2019. Effective preparation method of phosphopeptides from phosvitin and the analysis of peptide profiles using tandem mass spectrometry. J. Agric. Food Chem. 67:14086–14101.

Jie, Y. L., Z. X. Cai, S. S. Li, Z. Q. Xie, M. H. Ma, and X. Huang. 2017. Hydroxyapatite nucleation and growth on collagen electrospun

fibers controlled with different mineralization conditions and phosvitin. Macromolecular Res. 25:905–912.
Jie, Y., X. Li, Z. Cai, M. Ma, Y. Jin, D. U. Ahn, and X. Huang. 2018. Phosphorylation of phosvitin plays a crucial effects on the protein-induced differentiation and mineralization of osteoblastic MC3T3-E1 cells. Int. J. Biol. Macromolecules 118:1848–1854.
Kim, H. K., M. G. Kim, and K. H. Leem. 2014. Effects of egg yolk-derived peptide on osteogenic gene expression and mapk activation. Molecules 19:12909–12924.
Kim, H. S., M. Zheng, D. K. Kim, W. P. Lee, S. J. Yu, and B. O. Kim. 2018. Effects of 1,25-dihydroxyvitamin D-3 on the differentiation of MC3T3-E1 osteoblast-like cells. J. Periodontal Implant Sci. 48:34–46.
Korhonen, H., and A. Pihlanto. 2003. Bioactive peptides: novel applications for milk proteins. Appl. Biotechnol. Food Sci. Policy 1:133–144.
Kwak, S. Y., F. B. Wiedemann-Bidlack, E. Beniash, Y. Yamakoshi, J. P. Simmer, A. Litman, and H. C. Margolis. 2009. Role of 20-kDa amelogenin (P148) phosphorylation in calcium phosphate formation in vitro. J. Biol. Chem. 284:18972–18979.
Lee, H. Y., E. Abeyrathne, I. Choi, J. W. Suh, and D. U. K. Ahn. 2014. Sequential separation of immunoglobulin Y and phosvitin from chicken egg yolk without using organic solvents. Poult. Sci. 93:2668–2677.
Lee, S. H., and K. B. Song. 2009. Isolation of a calcium-binding peptide from enzymatic hydrolysates of porcine blood plasma protein. J. Korean Soc. Appl. Biol. Chem. 52:290–294.
Li, C., Y. Li, L. Zhang, S. Zhang, W. Yao, and Z. Zuo. 2019. The protective effect of piperine on ovariectomy induced bone loss in female mice and its enhancement effect of osteogenic differentiation via Wnt/beta-catenin signaling pathway. J. Funct. Foods 58:138–150.
Li, F., Y. Yang, P. Zhu, W. Chen, D. Qi, X. Shi, C. Zhang, Z. Yang, and P. Li. 2012. Echinacoside promotes bone regeneration by increasing OPG/RANKL ratio in MC3T3-E1 cells. Fitoterapia 83:1443–1450.
Lunenfeld, B., and P. Stratton. 2013. The clinical consequences of an ageing world and preventive strategies. Best Pract. Res. Clin. Obstet. Gynaecol. 27:643–659.
Mecham, D. K., and H. S. Olcott. 1949. Phosvitin, the principal phosphoprotein of egg yolk. J. Am. Chem. Soc. 71:3670–3679.
Mora, L., M. Reig, and F. Toldrá. 2014. Bioactive peptides generated from meat industry by-products. Food Res. Int. 65:344–349.
Quarto, M., C. Nitride, P. Ferranti, R. Mauriello, G. Garro, M. D. Stasio, M. G. Volpe, G. F. Ferrazzano, and L. Chianese. 2018. Peptidomic study on in vitro and in vivo phosphopeptide release during the chewing of gum fortified with a commercial casein hydrolysate. Int. Dairy J. 79:78–84.
Rachner, T. D., K. Sundeep, and L. C. Hofbauer. 2011. Osteoporosis: now and the future. Lancet 377:1276–1287.
Ren, J., Q. Li, M. Offengenden, and J. Wu. 2015. Preparation and characterization of phosphopeptides from egg yolk phosvitin. J. Funct. Foods 18:190–197.
Samaraweera, H., H. M. Sun, E. J. Lee, J. Grant, J. Fouks, I. Choi, J. W. Suh, and U. A. Dong. 2014. Characterisation of phosvitin phosphopeptides using MALDI-TOF mass spectrometry. Food Chem. 165:98–103.
Sritharan, S., T. P. Kannan, M. N. Norazmi, and A. A. Nurul. 2018. The synergistic effects of IL-6/IL-17A promote osteogenic differentiation by improving OPG/RANKL ratio and adhesion of MC3T3-E1 cells on hydroxyapatite. J. Cranio-Maxillofac. Surg. 46:1361–1367.
Tsuchita, H., T. Suzuki, and T. Kuwata. 2001. The effect of casein phosphopeptides on calcium absorption from calcium-fortified milk in growing rats. Br. J. Nutr. 85:5–10.
Udenigwe, C. C., and R. E. Aluko. 2012. Food protein-derived bioactive peptides: production, processing, and potential health benefits. J. Food Sci. 77:R11–R24.
Volk, S. P., D. U. Ahn, M. Zeece, and S. Jung. 2012. Effects of high-pressure processing and enzymatic dephosphorylation on phosvitin properties. J. Sci. Food Agric. 92:3095–3098.
Wallace, R. A., and J. P. Morgan. 1986. Isolation of phosvitin: retention of small molecular weight species and staining characteristics on electrophoretic gels. Anal. Biochem. 157:256–261.
Wang, X., A. Gao, Y. Chen, X. Zhang, S. Li, and Y. Chen. 2017. Preparation of cucumber seed peptide-calcium chelate by liquid state fermentation and its characterization. Food Chem. 229:487–494.
Wang, R. N., J. Green, Z. Wang, Y. Deng, M. Qiao, M. Peabody, C. Shen, A. Hu, R. L. Haydon, R. Kang, J. Mok, M. J. Lee, H. L. Luu, and L. L. Shi. 2014. Bone Morphogenetic Protein (BMP) signaling in development and human diseases. Genes Dis. 1:87–105.
Wang, Y., Y. H. Guo, X. P. Fan, F. J. Xiong, K. L. Wang, L. Z. Ma, and X. C. Jiao. 2018. Structure characterization of peptide chelating calcium derived from enzymatic hydrolysis of catfish flesh and bone paste. Sci. Technol. Food Industry 13:36–40.
Woo, J., T. Kwok, J. Leung, and N. Tang. 2009. Dietary intake, blood pressure and osteoporosis. J. Hum. Hypertens. 23:451–455.
Wu, D., R. Duan, F. Geng, X. Hu, N. Gan, and H. Li. 2020. Comparative analysis of the interaction of mono-, dis-, and tris-azo food dyes with egg white lysozyme: a combined spectroscopic and computational simulation approach. Food Chem. 284:180–187.
Wu, R. X., Q. Li, X. H. Pei, and K. F. Hu. , 2017. Effects of brucine on the OPG/RANKL/RANK signaling pathway in MDA-MB-231 and MC3T3-E1 cell coculture system. Evidence-Based Complement. Altern. Med. 2017:1–6.
Xia, G. H., S. S. Wang, M. He, X. C. Zhou, Y. L. Zhao, J. F. Wang, and C. H. Xue. 2015. Anti-osteoporotic activity of sialoglycoproteins isolated from the eggs of Carassius auratus by promoting osteogenesis and increasing OPG/RANKL ratio. J. Funct. Foods 15:137–150.
Zhao, G. L., Y. Liu, M. M. Zhao, J. Y. Ren, and B. Yang. 2011. Enzymatic hydrolysis and their effects on conformational and functional properties of peanut protein isolate. Food Chem. 127:1438–1443.
Zhong, Q., X. L. Li, W. D. Hu, B. Zeng, R. M. Liang, H. Liu, Z. X. Li, and Z. Zhang. 2016. Phosvitin phosphopeptide preparation using immobilised trypsin and enhancing calcium absorption in growing rats. Czech J. Food Sci. 34:325–331.